Hydrogen isotope accumulation in helium implantation zone in tungsten

S. Markelj[*a], T. Schwarz-Selinger[b], A. Založnik[a]

[a]*Jožef Stefan Institute (JSI), Jamova cesta 39, 1000 Ljubljana, Slovenia*
[b]*Max-Planck-Institut für Plasmaphysik (IPP), Boltzmannstrasse 2, D-85748 Garching, Germany*

Abstract

The influence of helium (He) on deuterium (D) transport and retention was studied experimentally in tungsten (W). Helium was implanted 1 μm deep into W to a maximum calculated concentration of 3.4 at.%. To minimize the influence of displacement damage created during the He implantation on D retention so-called self-damaged W was used. W was damaged by 20 MeV W ion bombardment and defects were populated by low-temperature D plasma at room temperature before He implantation. Deuterium depth profiling was performed in-situ during isochronal annealing in the temperature range from 300 K to 800 K. It is shown for the first time unambiguously that He attracts D and locally increases D trapping. Deuterium retention increased by a factor of two as compared to a non-He implanted W reference after sample annealing at 450 K. Rate equation modelling can explain the measured D depth profiles quantitatively when keeping the de-trapping parameters unchanged but only increasing the number of traps in the He zone. This bolsters the confidence in the theoretical calculations predicting that more hydrogen isotopes can be stored around a He cluster zone.

There is a lot of attention devoted to study the interaction of hydrogen isotopes (HIs) and He in metals since the presence of these light atoms influences the physical and mechanical properties of metals. To understand for example H- or He-embrittlement [1] their migration properties are of fundamental as well as practical interest. As one progresses towards realisation of a fusion reactor the influence of the presence of He on hydrogen isotope retention in plasma-exposed materials comes also into focus. In this case, He is either directly produced by the fusion reaction or indirectly by the decay of tritium or by transmutation of the wall materials. Recent experiments studying the interaction of HIs

and He with tungsten using He seeded D plasmas showed that He addition leads to reduced/supressed blistering [2,3] but forms nano-bubbles in the near surface layer [4]. Most importantly such microstructure leads to reduced D retention [2, 3, 5, 6]. The formation of nano-bubbles by few eV to keV He ion irradiation is fluence and temperature dependent, having a formation threshold around a fluence of 3×10^{20} He/m^2 at 290 K that is decreasing with the increase of temperature [4]. Similar nano-bubble formation but in larger depth was observed by MeV He ion irradiation where a fluence threshold of 10^{21} He/m^2 was obtained [7]. Annealing of 1.3 MeV He-irradiated samples with a fluence of more than 10^{21} He/m^2 up to 2273 K leads to pronounced surface blistering and exfoliation [7]. While there are several attempts to explain the reduced blistering and reduced D retention [2,3,4,5], the actual cause for these observations remains unclear. One possibility for the reduced retention is that implanted He might create a diffusion barrier for D transport [2]. Likewise, nano-sized bubbles might open-up additional pathways for D towards the surface thereby decreasing its transport into the bulk [3]. Contrary to these experimental findings density functional theory (DFT) calculations show strong attraction between He and HIs [8,9], indicating preferential trapping of H around He clusters. Molecular dynamics simulations show that a large amount of H can be accommodated around He bubbles [10]. Increased retention was found experimentally also in ion beam experiments. However, the challenge of these studies [11, 12, 13] is that the applied He and D implantation energies cause displacement damage which is known to increase retention in tungsten substantially. Hence, one cannot distinguish unambiguously the influence of the presence of He from the displacement damage that He causes.

The aim of the present work is to test the hypotheses of He acting as a diffusion barrier and inducing preferential binding of HIs around He. In order to study this unambiguously we took an alternative experimental approach. We tried to avoid the surface effects that nano-sized He bubbles might have on D retention by implanting He well below the surface. In order to decouple the influence of displacement damage created by He irradiation from the effect of the He-HIs interaction the study was made with so-called self-damaged tungsten produced by implantation of high energy W ions into W. The W ion implantation dose was chosen such that D retention would not increase any further with increasing ion damaging dose. Existing defects were decorated with D till D saturation was reached by gentle low-temperature plasma loading before He implantation. The possible effect of the implanted He zone acting as a diffusion barrier was studied by outgassing of D through the He implantation zone by annealing of the sample for 2 hours at individual temperatures in the temperature range between 300 K and 800 K, process called isochronal annealing. We expect that the He interaction is the same for all HIs due to the similar electronic structure, considering that the observed phenomena and theoretical calculations are not isotope dependent. We will mark by chemical symbols H and D when isotope composition is relevant.

Hot-rolled polycrystalline tungsten, manufactured by Plansee, with a purity of 99.997 wt. % was used in this study. Sample size was 12×15 mm^2, thickness 0.8 mm. It was chemo-mechanically polished to a mirror-like finish [14] and then heated for 2 min in ultra-high vacuum at 2000 K for re-crystallization. This procedure enlarges the grain size to 10 - 50 µm with (100) being the preferential grain orientation [14]. As all the annealing experiments presented here were conducted in-situ we could use one single sample thereby avoiding any influence of sample preparation.

After recrystallization, the sample was homogeneously irradiated by 20 MeV W ions to a fluence of 7.9×10^{17} W/m^2 in the TOF beam line of the tandem accelerator at IPP, Garching [15]. Using a displacement energy of 90 eV and evaluating the "vacancy.txt" output for the "Kinchin Pease" calculation option of the SRIM 2008.04 code [16] one obtains a peak damage level of 0.25 dpa [15]. A preceding study with the same material, damaging procedure and D loading showed that D retention saturates for a damage level well below this value [17]. In order to decorate the existing traps with D the sample was exposed to a well-characterized low-temperature D plasma [18] at 290 K at floating potential which results in an ion energy of < 5eV/D. A total D fluence of 1.5×10^{25} D/m^2 was accumulated over 72 h with a constant ion flux to the sample of 6×10^{19} D/m^{2}s. With this procedure we obtained a homogenous D depth profile within the first 2 µm with a D concentration of nearly 2 at. %. This initial D depth profile is shown in Fig 1 and marked as "Initial". The D depth profile was measured by D(^{3}He,p)α Nuclear Reaction Analysis (NRA) [19] in the centre of the sample just after the D exposure using a sequence of nine different ion beam energies from 500 keV to 4.5 MeV at the RKS setup of the tandem accelerator at IPP, Garching [15,20].

The final step of the sample preparation for the experiments was its irradiation by He ions at the TOF beam line at IPP, Garching [15]. One half of the sample (named further on in the text as "He half") was irradiated by 500 keV He ions with a fluence of 7.0×10^{20} He/m^2. According to SRIM this leads to a He peak concentration of 3.4 at. % in a depth of 0.84 µm with a FWHM of 0.29 µm, creating additional damage of 0.6 dpa at the damage peak in a depth of 0.76 µm. This He layer is located approximately in the middle of the W ion damage zone. The He depth profile and the damage dose profile induced by W ion bombardment as calculated by SRIM [16] are shown in Fig. 1. The other half (named further on in the text as "no-He half") of the sample was covered during He irradiation. When later on outgassing or D loading is performed on the whole sample, this procedure assures identical conditions for the He-irradiated and the no-He half and results can be directly compared.

After He-ion irradiation the sample was mounted in the INSIBA chamber at the tandem accelerator at JSI where isochronal annealing was performed. The set-up is described in more detail in

[21] and enables in-situ NRA measurements and heating of the samples up to 1200 K. Here, the sample was heated in temperature steps of 370 K, 450 K, 500 K, 550 K, 600 K, 700 K and 800 K, keeping the selected temperature constant for two hours. After each step the sample was cooled down and the NRA analysis was performed on the no-He and He-irradiated half of the sample in-situ by detecting protons from the $D(^3He,p)\alpha$ nuclear reaction. In order to determine the D depth profile [20] up to 7 μm, five different ^{3}He ion beam energies were used (0.73 MeV, 1.04 MeV, 1.55 MeV, 2.58 MeV, 4.32 MeV). We used the same collected charge of 7.45 μC for all five energies, corresponding to an ion dose of 4.65×10^{13} He$^+$ for the four lower energies and 2.3×10^{13} He^{2+} for the highest energy. The maximum ^{3}He concentration accumulated for each depth profile ranges between 0.08 at. % for the lowest energy and 0.02 at. % for the highest energy as calculated by SRIM [16]. In order to minimize any effect of the analysing ^{3}He ion beam on the no-He irradiated half, we changed the measurement position after two annealing temperatures.

Before the first annealing step a depth profile was measured on the He half at room temperature (RT) and was in good agreement with the profile shown in Fig. 1. The first annealing temperature was chosen to be 370 K. After 2 h of heating the sample was cooled down and the NRA proton signal was measured on both halves of the sample at the highest and the lowest ^{3}He beam energy. We observed no difference in the proton signals as compared to that obtained at RT. After the next step of 2 h sample heating at 450 K the proton signal was measured at all five ^{3}He beam energies. As expected, in the no-He half of the sample the D concentration dropped from initially 2 at.% to 1.3 at.%. On the contrary, pronounced accumulation of D in the He-implantation zone was observed, increasing the local D concentration from initially 2 at.% to 2.5 at.% as can be seen in Fig. 1. In other words the difference in the local D concentration at the depth of the He-implantation peak between the He-irradiated and the no-He half is a factor of two at 450 K. Although the strength of this study is that all experiments shown were conducted on one single sample out of scientific rigor the sequence was repeated on a second sample prepared and annealed in the same way and we observed the very same behaviour.

In Fig. 1 the comparison of D depth profiles for He and no-He half of the sample are shown for 450 K and 600 K together with the calculated He implantation profile. The increase of D concentration takes place at the depth were the calculated He implantation profile has its peak. The measured D concentration profile in this area is broader than the He-implantation profile due to the limited depth resolution of 0.5 μm at a depth of 1 μm. The integrated amount of D measured on the He half at RT, before start of the heating, was 2.1×10^{21} D/m^2. In the no-He half the integrated D amount decreased after heating at 450 K to 1.7×10^{21} D/m^2, which is 20 % less as compared to initial value obtained at RT.

4

The integrated D amount obtained in the He half at 450 K was 2.1×10^{21} D/m^2 and therefore the same as the total D amount obtained at RT. This implies that D that started to become mobile at 450 K did not diffuse out of the sample, as it was the case for the no-He half, but was redistributed to the He implantation zone.

With further temperature increase the D concentration started to decrease also in the He half of the sample, as is visible in Fig. 2 which shows the local D concentrations for both halves of the sample as a function of the annealing temperatures. The evolution of the local D concentrations between 0.5 µm and 1 µm as well as between 1.4 µm and 1.9 µm is plotted in Fig 2, indicated as zone 1 and zone 2 in Fig. 1, respectively. It can be seen in Fig. 1 and 2 that at 600 K D concentrations finally reach the same value for the no-He and the He half in a depth below 1 µm. In addition, D concentrations behind the He layer agree well with those in no-He half and drop in the same way. Hence no indication was found that He acts as a diffusion barrier. With further increase of temperature D concentrations in both halves continue to decrease. After the final heating to 800 K D concentrations in both halves of the sample reach the NRA detection limit.
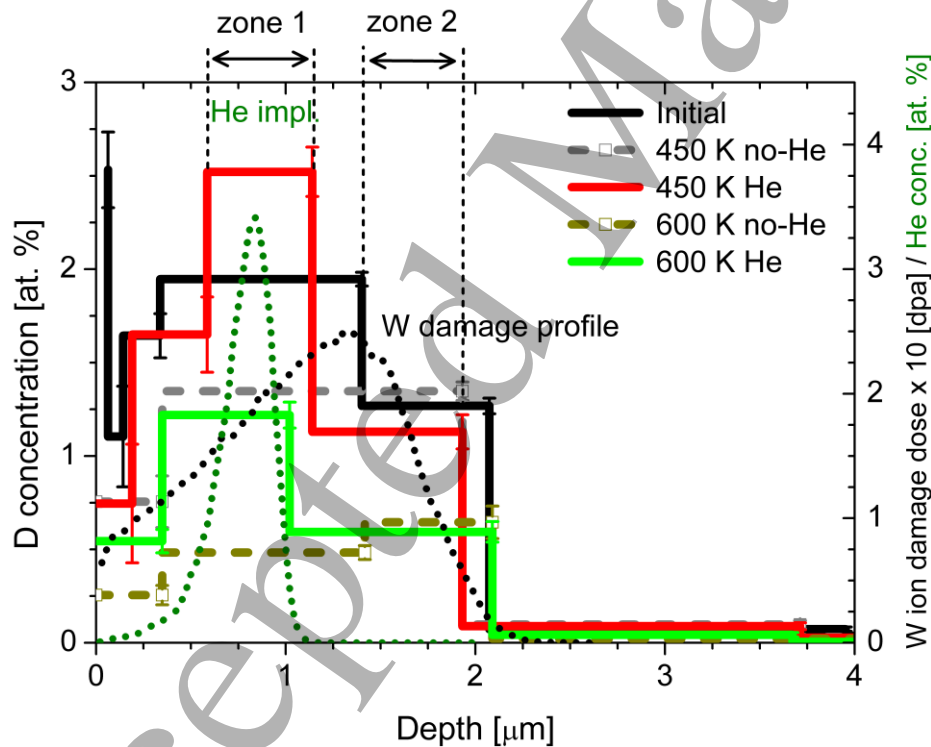

Figure 1: Comparison of D concentration depth profiles for no-He and He-irradiated half of the sample obtained after heating the sample at 450 K and 600 K for 2 hours. The green dotted line shows the He concentration profile as calculated by SRIM for 500 keV He ions, fluence 7.0×10^{20} He/m^2. Black dotted line is the depth profile of the damage dose as obtained by SRIM for 20 MeV W ion irradiation, fluence 7.9×10^{17} W/m^2.
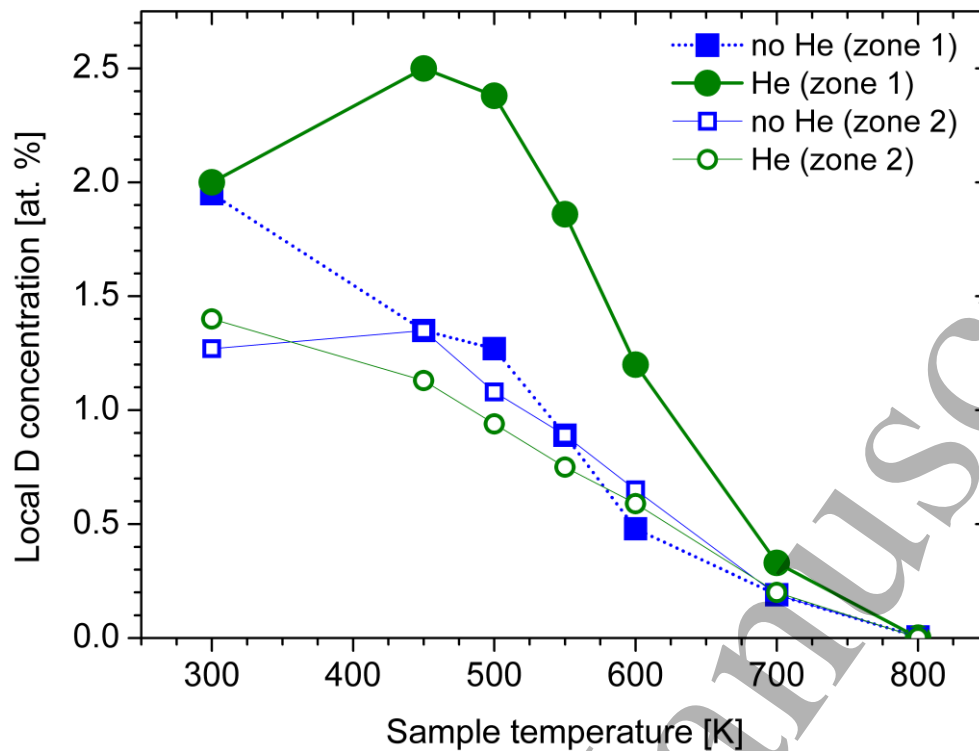
5

Figure 2: Local D concentrations for the two zones between 0.5 µm and 1 µm (zone 1) and between 1.4 µm and 1.9 µm (zone 2), see Fig. 1, as function of the annealing temperature for the no-He and the He-irradiated half of the sample.

With our approach to study the effect of He on D retention in the W lattice we avoided surface effects that He nano-bubbles might cause by moving the interaction zone 1 µm below the surface within a 2 µm deep zone of so-called self-damaged tungsten. Due to the large He mobility [9, 22] and attractive nature of He-He and He-vacancy [8, 9] in the W lattice, large He-vacancy clusters are probably formed in our damaged crystal lattice. Because the diffusivity of a He cluster or a He-vacancy cluster is suppressed [22, 23] we can assume He is accumulated in the implantation zone. The applied He fluence is still below the fluence where visible blisters would be formed on the surface [7]. This was also confirmed on a sample irradiated by 800 keV He to a fluence of 7.0×10^{20} He/m². Focused ion beam-cutting of the sample and analysing the cut by scanning electron microscopy showed indeed a different grey contrast in the He implantation zone, however, no nano-bubbles could be identified in depth.

During isochronal annealing we have observed strong accumulation of D around the He implantation zone. We observed that as soon as the pre-implanted D started to de-trap from the traps created by W ion irradiation it migrated to the He region where it was again trapped. On the no-He half a decrease of total D amount was observed. The influence of He-vacancy complex on H trapping and diffusion was studied in detail by density functional theory by Zhou et al. [9]. They found that the existence of He substantially affects the dissolution behaviour of interstitial H in the bulk of W. Namely,

6

H exhibits a lower solution energy around He being 0.76 eV, whereas the solution energy of H in the tetrahedral interstitial site (TIS) is 1 eV [9]. Moreover when adding a vacancy in such a system, He will be strongly trapped at the vacancy with a binding energy of 3-4 eV whereas the H trapping energy in a monovacancy is 0.8-1 eV [8]. Zhou et al. [9] also showed that when He is trapped in a vacancy there are more 'optimal charge density sites' for H (12 sites) as compared to a He-free vacancy (6 sites) due to the volume expansion. This suggests that He can serve as a trapping centre of H in the bulk. This observation could explain our observed increase of D concentration around the He implantation zone. Moreover when studying diffusion in such a complex, the standard diffusion barrier for H from TIS to TIS is 0.2 eV [9, 24, 25]. According to [9] the diffusion barrier and the solution energy are reduced when H is approaching the He-vacancy complex implying that H is attracted and will preferably bind there. Even though the calculation is made on the simplest possible complex - one H, one He atom, and one vacancy - one can speculate that this holds also for larger vacancy clusters and dislocation loops and lines filled with He atoms. It was shown by transmission electron microscopy [26] that W damaging by high energy W ion irradiation creates large density of dislocations and dislocation loops. He atoms will be trapped at such defects and will form He clusters due to the positive He-He binding energy in W [9]. If we assume that even larger He-vacancy complexes exhibit the same property of volume expansion as single He-vacancies complexes and hence providing more trap sites for D, we could explain our experimental observation. The binding energy of H does not depend much on the number of H and He present in a vacancy, being around 0.8-1 eV as calculated by DFT [8]. This holds also for larger vacancy-hydrogen-He (VHHe) clusters as was calculated in [27], where they have shown that the hydrogen trapping energy is not changed much by the presence of He in the clusters. This explains also why D eventually decreased in the He half with the same rate as in the no-He half and why D was below NRA detection limit on both halves of the sample at 800 K.

In order to verify if our data are compatible with the idea that addition of He into a vacancy increases only the number of binding sites for hydrogen atoms but keeps the de-trapping energy unchanged we applied the diffusion trapping code TESSIM [28]. Input parameters for the model were derived from a thermal desorption spectrum (TDS) of self-damaged tungsten prepared in an identical manner but loaded with D at a slightly higher temperature of 400 K [29], showing a D concentration of 1.5 at. % down to 2 μm [29]. TDS spectrum and D depth profile can be fitted with two trap types assuming a homogenous trap concentration for both trap sites down to 2 μm. In a recent study frequency factors and de-trapping energies were derived from the TDS peak shift applying different ramp rates [30, 31] to be $v_1 = 1.0 \times 10^{10}$ s^{-1}, $E_1^T = 1.0$ eV and $v_1 = 6.0 \times 10^{10}$ s^{-1}, $E_2^T = 1.5$ eV, respectively for samples from the same batch, prepared and D loaded in the same way. With trap concentrations of $C_1^T = 8.41 \times 10^{-3}$ at. fraction and $C_2^T = 6.59 \times 10^{-3}$ at. fraction and small variations in de-trapping energies $E_1^T = 0.93$ eV

7

and $E_2^T = 1.38$ eV one can describe the measured TDS spectrum. According to the desorption temperatures and de-trapping energies the traps could be attributed to vacancies and dislocation loops, respectively [32]. By implanting He in such a damaged crystal lattice, according to theory [9] the number of potential trapping sites doubles. The effect of additional traps sites created by the He was taken into account by doubling the number of traps for both sites in the He implantation zone centered at 0.84 µm. To be able to compare with our NRA depth profile we did not take the actual width from the SRIM calculation of 0.29 µm but spread these traps over a width of 0.58 µm due to lower NRA depth resolution. The simulation followed the same sequence as the experiment with individual temperatures held for 2 hours and cooling down in between the individual steps. In Fig. 3 the sum of the D retention in the individual traps are shown for the given temperatures after the sample was cooled down. The D concentration depth profile in the He zone changes very little after annealing the sample to 370 K. The depth profiles for each individual trap site (not shown) reveal that atoms from the low energy site populate the high energy site keeping the number of total D amount constant. At 370 K this can be observed only at the very edge of the implantation zone which is due to re-trapping of D atoms which have diffused outside the He region. When increasing the sample temperature to 450 K the D concentration increases in the He zone, identical to what was also observed in the experiment. Namely, D atoms de-trapped from low energy sites outside the He region, diffused and populated the available high energy sites in the He region. At 500 K D concentration drops slightly in the He zone also in agreement with the experiment, see Fig. 2. With further increase of the temperature the D concentration in the He zone starts to decrease, too. As in the experiment all D is desorbed at 800 K. Even though the simulation was intended to be of qualitative nature it even agrees quantitatively with the experiment especially in visualizing the trend of D concentration in the He zone.

Hence our experiment is in agreement with the assumption that the presence of He increases the number of trapping sites without modifying the de-trapping energy and hence we conclude there is an attractive potential between He and His. This result is especially important for theory since, as Cusentino et al. [33] pointed out, the choice of interatomic potential can substantially influence the results on hydrogen and He clustering behaviour. By experiment and modelling we have bolstered the confidence in existing theoretical calculations predicting that more HIs can be stored around a He cluster zone. This implies that reduced D retention observed in mixed He-D plasma experiments is not due to He acting as a diffusion barrier but might be a surface effect: possibly nano-sized bubbles open up additional pathways and enable HIs to diffuse back to the surface and decrease the transport to the bulk.
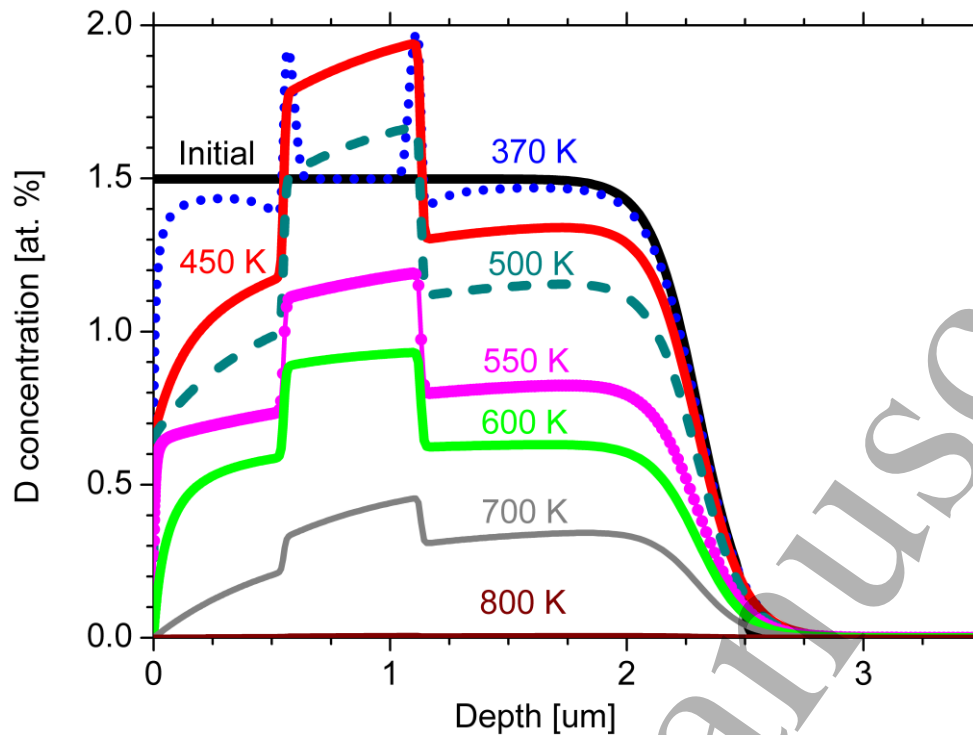
8

Figure 3: Simulated D concentration depth profiles after individual temperature steps assuming two trapping sites in the damaged region and increasing the concentration of trapping sites due to He presence in the He peak region with 0.58 µm wide constant profile centered at 0.84 µm.

Acknowledgments

9

References

[1] A. Pundt, R. Kirchheim, *Ann. Rev. Mater. Res.* **36**, 555-608 (2006)

[2] Y. Ueda et al. *J. Nucl. Mater.* 386-388, 725 (2009).

[3] V. Kh. Alimov et al. *Phys. Scr.* T138, 014048 (2009).

[4] M. Miyamoto et al. *J. Nucl. Mater.* 463, 333 (2015).

[5] M. J. Baldwin et al., *Nucl. Fusion* 51, 103021 (2011).

[6] H. T. Lee et al., *J. Nucl. Mater.* 415, S696–S700 (2011).

[7] S.B. Gilliam et al., *J. Nucl. Mater.* 347, 289 (2005).

[8] C.S. Becquart, C. Domain, *J. Nucl. Mater.* 386–388, 109 (2009).

[9] H-B. Zhou et al., *Nucl. Fusion* 50, 115010 (2010).

[10] N. Juslin and B. D. Wirth, *J. Nucl. Mater.* 438, S1221 (2013).

[11] H. Iwakiri, K. Morishita, N. Yoshida, *J. Nucl. Mater.* 307–311, 135 (2002).

[12] R. A. Causey, D.F. Cowgill, R. Doerner, R. Kolasinski, B. Mills, D. Morse, J. Smugeresky, W.R. Wampler, R. Williams, and D. Huber. *J. Nucl. Mater.* 415, S672 (2011):.

[13] I.I. Arkhipov, S. L. Kanashenko, V. M. Sharapov, R. Kh. Zalavutdinov, and A. E. Gorodetsky, *J. Nucl. Mater.* 363–365, 1168 (2007).

[14] A. Manhard, G. Matern, M. Balden*, Pract. Metallogr.* 50, 6 (2013) and A. Manhard, M. Balden, S. Elgeti, *Pract. Metallorg.* 52, 437 (2015).

[15] T. Schwarz-Selinger, PSI paper submitted to Nuclear Materials and Energy 2016

[16] J.F. Ziegler, www.srim.org.

[17] V. Kh. Alimov et al. *J. Nucl. Mater.* 441, 280 (2013).

[18] A. Manhard, T. Schwarz-Selinger, and W. Jacob, *Plasma Sources Sci. Technol.* 20, 15010 (2011).

[19] B. Wielunska, M. Mayer, T. Schwarz-Selinger, U. von Toussaint, and J. Bauer, *Nucl. Instr. and Meth. in Phys. Res. B* 371, 41 (2016).

[20] M. Mayer, E. Gauthier, K. Sugiyama and U. von Toussaint, *Nucl. Instr. and Meth. in Phys. Res. B* 267, 506 (2009).

[21] S. Markelj, A. Zaloznik, T. Schwarz-Selinger et al., *J. Nucl. Mater.* 469, 133 (2016) .

[22] C.S. Becquart and C. Domain, *Physical Review Letters* 97, 196402 (2006).

[23] P. Grigorev, D. Terentyev, G. Bonny, E. E. Zhurkin, G. van Oost, and J.-M. Noterdaeme, *J. Nucl. Mater.* 474, 143 (2016).

[24] K. Heinola and T. Ahlgren, *Journal of Applied Physics* 107, 113531 (2010).

[25] Y.-L. Liu, Y. Zhang, G.-N. Luo, and G.-H. Lu, *J. Nucl. Mater.* 390–391, 1032 (2009).

[26] A. Založnik, et al., *Phys. Scr.* T167, 014031 (2015).

[27] G. Bonny, P. Grigorev, and D. Terentyev, *Journal of Physics: Condensed Matter* 26, 485001 (2014).

[28] K. Schmid, V. Rieger, and A. Manhard, J. Nucl. Mater. 426, 247 (2012).

[29] E. Markina, M. Mayer, A. Manhard, and T. Schwarz-Selinger, J. Nucl. Mater. 463, 329 (2015).

[30] A. Manhard et al. in preparation

[31] M. Zibrov, S. Ryabtsev, Yu. Gasparyan, and A. Pisarev. *J. Nucl. Mater.* 477, 292 (2016).

[32] E. Hodille et al. 2017 and references therein, accepted in Nucl. Fusion

[33] M.A. Cusentino et al. *J Nucl Mater.* 463, 347 (2015).